

Microstructure reconstruction using entropic descriptors

BY RYSZARD PIASECKI^{*}

*Institute of Physics, University of Opole,
Oleska 48, 45-052 Opole, Poland*

Simulated annealing based a new approach to the inverse reconstruction of a pattern's microstructure is reported. Instead of a variety of correlation function, a pair of entropic descriptors for average inhomogeneity and statistical complexity is used. They reveal structural information that is dissimilar at least in part to that given by correlation functions at almost all discrete length scales. The method has been tested on surrogate binary and greyscale images. In each of the cases the persuasive realization of their microstructure is obtained.

Keywords: Microstructure reconstruction; entropic descriptors; statistical complexity

1. Introduction

“To what extent can the structure of a disordered heterogeneous material be reconstructed using limited but essentially exact structural information about the original system?” – the first sentence of the abstract in [Rintoul & Torquato \(1997\)](#) still remains a vital question of modelling heterogeneous materials. Much research effort has been concentrated on this topic. One of the particularly useful is the simulated annealing (SA) technique, widely discussed in [Torquato \(2002a, b\)](#) and [Jiao *et al.* \(2007, 2008\)](#). This technique has the advantage that it is developed for problems with many local minima. The simplest SA-reconstruction of a digitized microstructure by [Yeong & Torquato \(1998a\)](#) makes use of the two-point correlation function $S_2(r)$ that represents the probability of finding two particles (pixels) of the phase of interest separated by a distance r . Another concept based on incorporating the fast Fourier transform algorithm to calculate S_2 , as developed in [Cule & Torquato \(1999\)](#) and [Fullwood *et al.* \(2008a, b\)](#), results in very close replicas of regular and more varied two-phase microstructures up to a translation. On the other hand, [Kumar *et al.* \(2006\)](#) clearly stated: “the reconstruction process is not meant to exactly duplicate the parent (target) microstructure, which is already at hand, but rather to create statistically similar microstructures...”. Very recently, a genetic algorithm and maximum entropy method has been compared with SA and a *hybrid* approach based on genetic algorithms and SA has been proposed by [Patelli & Schuëller \(2009\)](#).

The SA proceeds to find a statistically reasonable realization by evolving the microstructure in such a manner that minimizes ‘energy’ function E taken as squared difference between the correlation functions of the target (reference) and trial (generated) patterns. For isotropic media this is a quite effective approach except the dense systems with significant aggregation of the particles like the sticky-disk model of [Rintoul & Torquato \(1997\)](#) or multiscale patterns in [Jiao *et al.* \(2008\)](#). Such structurally complex systems show characteristic features at certain length scales. The [Jiao *et al.* \(2008\)](#) S_2 -reconstruction of a binary (black and white) complex laser-speckle pattern revealed that the $S_2(r)$ alone could not capture in a satisfactory way all its

^{*} E-mail address: piaser@uni.opole.pl

structural features. Due to the limited information contained in a single correlation function, the reconstructed microstructure was not unique. In general, a multiscale structure cannot be fully characterised with a single lower-order correlation function; see [Yeong & Torquato \(1998a\)](#). The situation becomes more satisfactory when the second correlation function, e.g., the lineal-path function $L(r)$ studied in [Lu & Torquato \(1992\)](#) is also included in a hybrid reconstruction procedure ([Yeong & Torquato 1998a](#); [Torquato 2002a, b](#); [Kumar et al. 2006](#); [Jiao et al. 2007, 2008](#)). By evaluation of the probability of finding an entire line segment of length r within the phase of interest, the $L(r)$ gives information such as the lineal clustering or a coarse level of the connectedness of the microstructure.

Motivated by these observations, certain entropic descriptors ([Piasecki 2000a, b, 2009a](#); [Piasecki & Plastino 2010](#)) are employed for the first time to innovative reconstruction of a pattern's microstructure. The entropic descriptors (EDs) are able to detect relatively dissimilar pattern's features (cf. [figure 5](#) in [Piasecki 2009b](#)) compared to S_2 -correlation function. The unbiased hybrid reconstruction (UHR) method we propose provides encouraging results not only for binary (0-1) images. In contrast to correlation functions, the UHR method is with no trouble applicable also to complex greyscale (0-255) images. Thus, a fresh view is created in the context of reconstructing random media for predicting their effective physical properties and performance optimization; see the recent reviews of [Wang & Pan \(2008\)](#) and [Fullwood et al. \(2009\)](#).

In this paper, I would like to concentrate on the specific and novel application of EDs, i.e., microstructure reconstruction, not on the other possible categories of spatio-compositional inhomogeneity or spatio-compositional complexity. The introduction to those broad topics can be found in the two latest articles ([Piasecki 2009b](#), [Piasecki & Plastino 2010](#)). This is a reason why only the list of the appropriate formulas and the most important details are given in [Appendix](#). The rest of this paper is organized as follows. In Section 2 the different entropic descriptors are briefly introduced. Next, in Section 3 the basic versions of the UHR method are formulated and described. Then, the method is examined on some examples of surrogate patterns in Section 4. Section 5 is devoted to final conclusion and suggestion on further development of the hybrid approach.

2. Entropic descriptors

In the simplest version, the proposed hybrid reconstruction of a binary pattern needs the ED-pair $\{S_\Delta; C_\lambda(S)\} \equiv \{S_\Delta; C_{\lambda, S}\}$ of an average (per cell) *spatial* inhomogeneity introduced in [Piasecki \(2000a, b\)](#) and *spatial* statistical complexity considered by [Piasecki & Plastino \(2010\)](#), respectively. The second ED-pair we use is $\{S_{\text{gr}, \Delta}; C_\lambda(S_{\text{gr}})\} \equiv \{G_\Delta; C_{\lambda, G}\}$ and basically relates to greyscale images. Now, the G_Δ -component quantifies an average grey level inhomogeneity ([Piasecki 2009a, b](#)), the so-called *compositional* inhomogeneity. The $C_{\lambda, G}$ -part quantifies an average grey level statistical complexity ([Piasecki & Plastino 2010](#)), the so-called *compositional* statistical complexity. The all descriptors make the use of microcanonical entropy $\text{Entr} = k_B \ln \Omega$, where k_B is equal to unity and Ω denotes the number of microstates realizing a macrostate properly defined; see also [Appendix](#).

A configurational (binary) macrostate can be simply described with the help of the order dependent set of cell occupation numbers $\{n_i(k)\}$, $i = 1, 2, \dots, \kappa(k)$, of black pixels (finite size 1×1 -objects) inside i th sliding sampling cell of size $k \times k$. The side length of the cell defines the discrete length scale k . Here $\kappa(k) = [L - k + 1]^2$ is the length scale depending number of allowed positions of the sliding cell (with maximal overlapping) for a given pattern of size $L \times L$. In turn, the set of i th cell sums $\{g_i(k)\}$ of grey level values determines a compositional (grey level) macrostate. Notice that for the latter case all possible order dependent partitions,

allowing some of the parts to be zero, of $g_i(k)$ over k^2 unit cells inside i th cell is referred to as a *weak* composition (Stanley 2001); additional details can be found in Piasecki (2009a, b).

In our approach, for any length scale $1 \leq k \leq L$ the binary S_Δ -component [the grey level counterpart G_Δ] of the ED-pairs takes into account the statistical *dissimilarity* of actual (current) macrostate $AM(S)$ [$AM(G)$] and reference (theoretical) one $RM_{\max}(S)$ [$RM_{\max}(G)$] that maximizes appropriate entropy. Thus it is natural to consider the difference of the corresponding entropies. The general form for the entropic binary descriptor reads therefore

$$S_\Delta(k) = \frac{[Entr_{\max}(S) - Entr(S)]}{\kappa}, \quad (2.1)$$

while for the grey level case

$$G_\Delta(k) = \frac{[Entr_{\max}(G) - Entr(G)]}{\kappa}. \quad (2.2)$$

To simplify the notation the variable k is omitted on the right-hand side of equations 2.1-2.4. For a given pattern the averaging procedure allows one to compare the descriptor values at different length scales k . Of course, for a given binary [greyscale] pattern the form of entropy in equations 2.1-2.4 should be specified adequately to each case. Here only the main idea of the EDs is presented. The more detailed description can be found in Piasecki (2000a, b; 2009a, b). However, to increase an accessibility of the present method, the formulas used for computing of the numbers Ω of realizations of appropriate macrostates are given in Appendix.

Consecutively, the binary $C_{\lambda,S}$ -component of the ED-pairs takes into consideration the statistical *dissimilarity* of macrostates in the pairs: $AM(S)$ and $RM_{\max}(S)$, $AM(S)$ and $RM_{\min}(S)$, $RM_{\max}(S)$ and $RM_{\min}(S)$, and in the similar way for the grey level counterpart $C_{\lambda,G}$. In particular, we are interested in those structural features that depend on the length scale k . This type of entropic descriptor is able to distinguish structurally distinct configurational (compositional) macrostates with identical or nearly the same degree of spatial (compositional) disorder. The general form of the entropic binary descriptor is given by

$$C_{\lambda,S}(k) = \frac{1}{\kappa} \frac{[Entr_{\max}(S) - Entr(S)][Entr(S) - Entr_{\min}(S)]}{[Entr_{\max}(S) - Entr_{\min}(S)]}, \quad (2.3)$$

while for the grey level case

$$C_{\lambda,G}(k) = \frac{1}{\kappa} \frac{[Entr_{\max}(G) - Entr(G)][Entr(G) - Entr_{\min}(G)]}{[Entr_{\max}(G) - Entr_{\min}(G)]}. \quad (2.4)$$

For any length scale k each of the above statistical complexities vanishes for the two opposite extremes: (I) the corresponding maximum inhomogeneity, when $Entr \rightarrow Entr_{\min}$, and (II) the corresponding maximum homogeneity, when $Entr \rightarrow Entr_{\max}$. In between these two special instances, the highest value of spatial or compositional statistical complexity exists: $C_{\lambda,\max}(\Omega)|_{\Omega=\Omega_0} = [\ln(\Omega_{\max}/\Omega_{\min})]/4\kappa$ for $\Omega_0 = (\Omega_{\max}\Omega_{\min})^{1/2}$ given here in rather enlightening Ω -notation. In pattern's language, the most statistically complex arrangement at a given length scale emerges when the average *departure* of the actual entropy $Entr$ from its maximum possible value $Entr_{\max}$ is comparable to that from its minimum possible value $Entr_{\min}$ (Piasecki & Plastino 2010). Further details can be found in Piasecki & Plastino (2010).

3. The unbiased hybrid reconstruction

Let us denote by $S_{\Delta}^0(k)$ [$G_{\Delta}^0(k)$] and $C_{\lambda,S}^0(k)$ [$C_{\lambda,G}^0(k)$] the binary [greyscale] *target* entropic descriptors computed at a given length scale k . Their counterparts, i.e., the EDs for *trial* patterns will be marked by the corresponding symbols without the superscript zero. Within the present approach the aforementioned energy function can be taken in any of its hybrid forms $E \equiv E_j$, where $j = S, G$ and M . As before the ‘ S ’ and ‘ G ’ refer respectively to a binary and greyscale image while the ‘ M ’ relates to a binary pattern that is encoded in two ways: (a) the standard one (0 = black, 1 = white) and (b) the greyscale fashion (0 = black, 255 = white). Instead of two target EDs, the latter ‘two-fold’ encoding incorporates the set of four EDs. This allows for obtaining a higher structural accuracy in the simulation procedure – for a given tolerance δ -value mentioned below – in comparison to that obtained by means of only two target EDs. This technique has been used in a one of the numerical examples; see the related [figure 4a](#).

The E_j can be expressed as the weighted, by the parameter $1/m$, sum of squared differences between target entropic descriptors and those computed for trial configurations

$$E_j = \frac{1}{m} \sum_{k=1}^L \varepsilon_j(k), \quad (3.1)$$

where $m = 2$ for instances given by [equations 3.2](#) and [3.3](#), and $m = 4$ for [equation 3.4](#) is the number of different EDs. The length scale depending terms $\varepsilon_j(k)$ in [equation 3.1](#) are specified as

$$\varepsilon_S(k) = [(S_{\Delta} - S_{\Delta}^0)^2 + (C_{\lambda,S} - C_{\lambda,S}^0)^2], \quad m = 2 \quad (3.2)$$

$$\varepsilon_G(k) = [(G_{\Delta} - G_{\Delta}^0)^2 + (C_{\lambda,G} - C_{\lambda,G}^0)^2], \quad m = 2 \quad (3.3)$$

and

$$\varepsilon_M(k) = \varepsilon_S(k) + \varepsilon_G(k), \quad m = 4. \quad (3.4)$$

Considering every configuration as a ‘state’ of the system, E can be described as a function of the states; cf. [Jiao et al. \(2007\)](#) for S_2 -reconstruction.

Now, to minimise an objective function E we repeat the following steps. For a current configuration of binary [greyscale] pattern two randomly selected pixels of different phases [different grey levels] are interchanged giving the new trial state. The new configuration is then accepted with probability $p(\Delta E)$ given by the Metropolis acceptance rule, see its description in [Torquato \(2002a\)](#),

$$p(\Delta E) = \begin{cases} 1 & \Delta E \leq 0, \\ \exp(-\Delta E/T), & \Delta E > 0, \end{cases} \quad (3.5)$$

where $\Delta E = E_{\text{new}} - E_{\text{old}}$ is the change in the energy between the two successive states. Upon acceptance, the trial pattern becomes a current one, and this simple evolving procedure is repeated. The variation of a fictitious temperature T as a function of time is called the cooling schedule associated with the annealing process. We use the popular cooling schedule $T(l)/T(0) = \gamma^l$ with a positive parameter $\gamma = 0.8$, where l numerates annealing steps. Note that if the thermalisation (the system should evolve long enough at $T(l)$) and annealing rate (the closer γ to one the slower annealing process) are not carefully chosen then one can obtain suboptimal results. However, for practical test purposes, the above cooling schedule is

sufficient (Jiao *et al.* 2007). We terminate the reconstruction when E becomes smaller than a given tolerance value δ . Here, the distinct δ -values were chosen in order to avoid a considerable increase in computation time that depends mainly on the pattern's size and also on the type of hybrid approach. It should be stressed that in the later stages of SA no special technique, as discussed in Jiao *et al.* (2008) and Kumar *et al.* (2006), requiring the use of a biased pixel-selection process or modifying the exchange of isolated pixels in either of the phases has been used. Therefore the proposed approach belongs to the *unbiased* annealing technique.

4. Illustrative examples

The capability for reconstruction of various microstructures by the proposed UHR method is examined on the following examples of surrogate patterns.

Example 4.1. First we consider a binary target pattern of size 36×36 ; see the inset T #1 in figure 1a. For testing purposes, this synthetic pattern is created by means of a cellular automata-like model. The optimization procedure was started with an initial configuration of white and black pixels in a random checkerboard arrangement at a prescribed volume fraction $(664/36^2) \cong 0.5123$ of black phase. Finally, the UHR procedure has been terminated when $E \leq \delta = 4 \cdot 10^{-4}$. Such a tolerance value, notwithstanding the usage of only one pair of spatial EDs, in this case the $\{S_\Delta, C_{\lambda, S}\}$, yields a structurally convincing target pattern's reconstruction as depicted in the inset R #1 in figure 1a. Only a few isolated pixels appear. The lines and symbols refer to appropriate ED computed for the target pattern T #1 and its reconstruction R #1, respectively. It is instructive to consider the behaviour of two-point correlation function S_2 of black phase. For simplicity, it is evaluated along two orthogonal directions (the rows and columns of pixels); see figure 1b. This orthogonal-sampling algorithm introduced by Yeong & Torquato (1998a, b) was applied to the patterns T #1 (solid line) and R #1 (dashed line). We use this kind of simplified S_2 -evaluation as well as the hard-wall conditions also for next figures.

The small δ -value ensures, as shown in figure 1a, well fitting both target ED-curves with the corresponding symbols for the reconstructed pattern at every length scale k . However, the S_2 -counterparts, solid line for T #1 and dashed one for R #1, display in figure 1b the comparable behaviour only at initial length scales. An analogous behaviour can be also observed in subsequent figures 2b, 3b and 4b, which correspond to more diversified arrangements. Thus it appears clear that limited structural information provided by correlation function S_2 and on the other hand, by entropic descriptors is comparatively different (at least in part) at almost all discrete length scales. Earlier, such possibility was signaled by the reverse discrepancy, i.e., between S_Δ -curves as well as G_Δ -lines. It was revealed for the two adapted patterns (cf. figure 5 in Piasecki 2009b): the “initial” one related to target laser-speckle pattern and its S_2 -reconstruction obtained by Jiao *et al.* (2008).

Additionally, in figure 1c this kind of behaviour is enlightened from a different viewpoint. Namely, for the method of sliding sampling cell the so-called *auxiliary* patterns play important role at every length scale k ; for more details see Appendix. Since the first maximum of both EDs appears at length scale $k_{\max} = 6$ we choose it as the most characteristic scale. Then, the size of related ‘representative’ patterns, auxT #1 and auxR #1, equals to $(L - k_{\max} + 1) k_{\max} = 186$. In figure 1c both S_2 -curves, solid line for auxT #1 and dashed one for auxR #1, exhibit now oscillations with periodicity roughly equal to the length scale we consider. This kind of a spatial correlation is primarily due to the way we create the

representative patterns. Nevertheless, once more the larger length scale k the larger discrepancies are between the two S_2 -curves.

Examples 4.2 & 4.3. Consider now a modified 42×42 domain of greyscale image adapted from [Noussiou & Provata \(2007\)](#). There a surface reconstruction in reactive dynamics within mesoscopic kinetic Monte Carlo approach was performed. For testing reasons we convert the domain into a three-level ($255 = \text{white}$, $127 = \text{grey}$ and $0 = \text{black}$) target pattern T #2 by specifying two greyscale thresholds, which lead to the equal volume fraction $(588/42^2) \cong 0.333$ of white, grey and black phases; see the inset in [figure 2a](#). The connotation of each of the colours is irrelevant here, as it has nothing to do with the purposes of the UHR presentation. It is worth noticing that the most compact clusters form black pixels. Keeping unchanged distribution of the black phase and interchanging the more spread-out white with the grey phase, one additional target pattern T #3 is created for further comparison; see the inset in [figure 3a](#). Since for simulation results the influence by itself of the volume fraction of each phase is exactly the same for both patterns T #2 and T #3, only the structural differences between arrangements of white and grey pixels are expected to be responsible for the varieties of behaviour of EDs.

In both cases the UHR procedure is started from the identical random configurations of black, grey and white pixels. It has been terminated using the same tolerance value $\delta = 4 \cdot 10^{-4}$. The usage of a one pair of compositional EDs, this time the $\{G_\Delta, C_{\lambda, G}\}$, yields again structurally persuasive realizations of the target patterns; see the insets R #2 and R #3 in [figures 2a](#) and [3a](#). The corresponding curves (and symbols) show the latter case as having slightly higher compositional inhomogeneity and statistical complexity than the former one. The detection of such subtle effect by the naked eye inspection of the patterns seems to be impossible. Thus, the UHR approach employing merely one pair of proper EDs is still a useful tool even for multiphase media.

To compare the UHR with the correlation function approach, in [figures 2b](#) and [3b](#) from top to bottom, the orthogonal S_2 -function of a white, grey and black phase is shown for T #2 and T #3 (solid lines), R #2 and R #3 (dashed lines). The S_2 -values are presented within the most interesting range. As is easily seen in [figures 2b](#) and [3b](#), despite of small error tolerance δ , the corresponding pairs of S_2 shown lack of similarity over nearly all of length scales. Again one can take for granted that correlation function S_2 and entropic descriptors provide relatively dissimilar structural information.

Example 4.4. The UHR method is examined now for the complex binary laser-speckle pattern that belongs to a class of multiscale patterns. A 64×64 sub-domain (upper left corner) was adapted from 129×129 -version of the target pattern (cf. [figure 12a](#) in [Jiao *et al.* 2008](#)) and denoted here as T #4. Making use of the already mentioned two-fold encoding of a binary pattern, the two ED-pairs, $\{S_\Delta, C_{\lambda, S}\}$ and $\{G_\Delta, C_{\lambda, G}\}$, contribute in this instance. The UHR procedure has been terminated when $E \leq \delta = 2 \cdot 10^{-2}$; see [figure 4a](#), where as usually the lines and symbols correspond to target pattern T #4 and its reconstruction R #4, which are depicted in the insets of [figure 4b](#).

Let us make the preliminary comparison with the four non-overlapping 64×64 sub-domains A, B, C and D (see [Table 1](#)) of the S_2 -reconstruction of the whole 129×129 target pattern (cf. [figure 13](#) in [Jiao *et al.* 2008](#)). The present method clearly yields structurally persuasive realization R #4 of the target pattern T #4. Additionally, the two-point correlation S_2 -function of black phase computed by orthogonal-sampling algorithm for these patterns, T #4 (solid line) and R #4 (dashed line) clearly indicates that limited structural information given by the correlation function differs in part from that obtained with entropic descriptors;

see [figure 4b](#). It is worth noticing that the number n_1 of isolated black pixels for the R #3-reconstruction ($n_1 = 67$) is much closer to that for the target pattern T #3 ($n_1 = 69$), see [figure 4c](#), in comparison to the four sub-domains: A ($n_1 = 48$), B ($n_1 = 51$), C ($n_1 = 81$) and D ($n_1 = 75$) given in [Table 1](#). In addition, there the numbers of clusters of other sizes for the chosen sub-domains are specified. One can state that multiscale structural elements like the small black clusters and black stripes are reconstructed in a satisfactory way by the present UHR method. However, we should remember that a suitable comparison between the S_2 -reconstruction and the UHR-method needs a re-examination of the latter one for the whole target pattern of size 129×129 .

Table 1. The number $n(s)$ of cluster sizes s (measured in pixels) for the target pattern T #4 and its UHR-reconstruction R #4. Additionally, for preliminary comparison purposes the number $n(s)$ for the four non-overlapping 64×64 sub-domains marked here as $\begin{smallmatrix} AB \\ CD \end{smallmatrix}$ is given. The exemplary sub-domains are taken from S_2 -reconstruction obtained by [Jiao et al. \(2008\)](#). Each of the patterns is depicted below the appropriate column.

T #4		R #4		A		B		C		D	
s	n	s	n	s	n	s	n	s	n	s	n
1	69	1	67	1	48	1	51	1	81	1	75
2	13	2	26	2	10	2	2	2	8	2	9
3	12	3	11	3	6	3	6	3	4	3	3
4	4	4	6	4	1	4	2	4	3	4	6
5	1	5	3	5	1	5	1	5	4	5	1
6	2	6	4	6	2	6	1	6	4	7	2
7	1	7	3	7	2	7	1	7	3	8	1
9	2	11	1	8	1	8	1	9	2	12	1
10	1	16	1	13	1	10	1	10	1	13	1
12	1	18	1	14	1	11	1	11	1	14	2
32	1	20	1	23	1	16	1	12	2	18	1
55	1	38	1	34	1	25	1	17	1	22	1
58	1	51	1	101	1	2593	1	18	1	24	1
60	1	62	1	424	1			19	1	27	1
75	1	88	1	1950	1			29	1	2284	1
2155	1	257	1					33	1		
		1849	1					2085	1		



Example 4.5. Now focus on a fully grey level pattern. Avoiding mathematical details, which are not a subject of the present work, a greyscale pattern without a clear symmetry (see the accompanying animation) is adapted from [Rucklidge & Silber \(2009\)](#). The pattern is a transient one between the 12-fold and 14-fold approximate quasipatterns. The authors have investigated the time-dependent model partial differential equation involving the pattern-forming field $U(x, y, t)$ being a complex-valued function and real-valued 2π -periodic forcing function $f(t)$; cf. [equation \(3.1\)](#) in [Rucklidge & Silber \(2009\)](#). In resulting patterns the greyscale represents the real part of $U(x, y, t)$. In order to reduce the computation cost, the 137×137 sub-domain exemplary for the transient case was resized to 69×69 . This modified greyscale pattern is chosen as the target one T #5; see the middle inset in [figure 5b](#). The UHR procedure using one pair of compositional EDs, $\{G_A, C_{A,G}\}$, was started with an initial random configuration I #5 having the same grey level histogram as T #5. It has been terminated when $E \leq \delta = 3 \cdot 10^{-5}$. In [figure 5a](#), the solid G_A -line and symbols refer to target

pattern T #5 and its reconstruction R #5. For comparison, the dashed line corresponding to I #5 is also shown. The inset in [figure 5a](#) shows that the $C_{\lambda, G}$ -line is hardly distinguishable from the G_A -one even around the first peak and therefore it is absent on the main part of [figure 5a](#). Similarly to the earlier examples, one can observe that the UHR method applied to entirely greyscale pattern still permits for structurally credible its reconstruction. This supports belief that the present approach is quite universal one although relatively time consuming. On a standard personal computer the number of MC steps needed, e.g., in the case of multiscale laser-speckle binary pattern equals to about $2 \cdot 10^5$. Increasing the efficiency of the program code this number could be twice reduced approximately. However, to obtain statistically significant number of reconstructions, especially for patterns larger in size, it is crucial the use of a more powerful computer.

5. Conclusions

We gather that the unbiased hybrid reconstruction approach is generally applicable to a wide class of digitized media. This observation is supported by other microstructure reconstructions for a variety of patterns not yet presented here. The main conclusion to be drawn can be summarized as follows: the microstructural information revealed by means of the entropic descriptors allows for innovative reconstruction of every type of binary and grey level patterns. The most of multiscale structural elements is reconstructed on an acceptable level in connection with an assumed tolerance δ -value. It is worth noticing that the proposed versatile method can be extended to q -entropies ([Piasecki et al. 2002](#)) that are being the subject of much work in statistical mechanics ([Tsallis 2009](#)).

Finally, after the main part of this paper was completed the author became aware of [Jiao et al. \(2009\)](#) article, where the hybrid $\{S_2(r); C_2(r)\}$ -reconstruction was tested successfully on textures drawn from material science, cosmology and granular media. The approach incorporates a promising descriptor of random textures, i.e., the two-point cluster function $C_2(r)$ developed in [Torquato et al. \(1988\)](#). A cluster of phase i is defined as the part of phase i that can be reached from a point in phase i without passing through phase $j \neq i$ ([Torquato 2002b](#)). This function gives the probability of finding two points separated by a distance r in the same cluster of the phase of interest. Thus it can serve as a sensitive structural indicator when clustering and phase connectedness appear. One can envisage a simple way of further improving of the reconstruction process. For instance, any of the entropic descriptors can be easily combined with the two-point cluster function. Complementary structural information, although limited, should be probably captured by means of this sort of a hybrid approach.

Acknowledgements

I would like to thank Angelo Plastino for careful reading an earlier version of this paper and Wiesław Olchawa for providing clusters distribution procedure.

Appendix

In general, given binary (S) or grey level (G) pattern of size $L \times L$ can be sampled by $\kappa(k) = [(L - k)/z + 1]^2$ cells of size $k \times k$ with a sliding factor $1 \leq z \leq k$ provided $(L - k) \bmod z = 0$. Here the $z = 1$ is chosen that gives the maximal overlapping of the cells. In fact, in this way we analyse auxiliary patterns $L_a(k) \times L_a(k)$, where $L_a(k) \equiv [(L - k)/z + 1] k$. Those patterns composed of the sampled cells placed in a non-overlapping manner can be treated as the representative ones since they clearly reproduce the general structure of the initial images. Such approach allows us to compute the reference entropies, $Entr_{\max}$ and $Entr_{\min}$, which are related to specific macrostates of the representative patterns. Keeping this in mind, the basic constraints at every length scale k for cell occupation numbers $n_i(k)$ and for local grey level sums $g_i(k)$ can be written as:

$$(i) \quad \sum_{i=1}^{\kappa} n_i(k) = N(k), \quad (ii) \quad \sum_{i=1}^{\kappa} g_i(k) = G(k), \quad (A.1)$$

where $N(k)$ and $G(k)$ stand for the length scale depending total number of black pixels and total sum of grey level values, respectively. We assume that the black pixels concentration $\varphi_S = N(k)/\kappa k^2$ as well as the normalized average (per cell) sum of grey level values $\varphi_G = G(k)/255 \kappa k^2$ are non-trivial. That means the following inequalities are obeyed: $0 < \varphi_S < 1$ and $0 < \varphi_G < 1$. To simplify notation we will omit the parameter k wherever it does not lead to misunderstanding.

At every fixed length scale k , only the numbers of realizations of appropriate macrostates are listed below. The first three of them, i.e., [equations A.2-A.4](#), refer to binary patterns and the remaining ones, i.e., [equations A.5-A.7](#), relate to grey level case. We begin with the clear number $\Omega(S)$ of realizations of the actual macrostate $AM(S)$ that is the product of the ways that each of sampled cells composed of k^2 unit cells can be occupied with the number n_i of black pixels under above constraint (i)

$$\Omega(S) = \prod_{i=1}^{\kappa} \binom{k^2}{n_i}. \quad (A.2)$$

The maximum possible value $Entr_{\max}(S)$ is accessible for most spatially homogeneous reference macrostate, $RM_{\max}(S) \equiv \{n_i \in (n_0, n_0 + 1)\}_{\max}$, with $\kappa - r_0$ and r_0 number of cells occupied by $n_0 \in (0, 1, \dots, k^2 - 1)$ and $n_0 + 1$ of black pixels. Thus, the simple relation holds: $N = (\kappa - r_0)\{n_0\} + r_0\{n_0 + 1\} \equiv \kappa n_0 + r_0$, where $r_0 = N \bmod \kappa$, $r_0 \in (0, 1, \dots, \kappa - 1)$ and $n_0 = (N - r_0)/\kappa$. The number of proper microstates then reads

$$\Omega_{\max}(S) = \binom{k^2}{n_0}^{\kappa - r_0} \binom{k^2}{n_0 + 1}^{r_0}. \quad (A.3)$$

In turn, the minimum possible value $Entr_{\min}(S)$ is available for most spatially inhomogeneous reference macrostate, $RM_{\min}(S) \equiv \{n_i \in (0, n, k^2)\}_{\min}$, with $\kappa - q_0 - 1$ of empty cells, one cell with $n_i = n \in (0, 1, \dots, k^2 - 1)$ and q_0 of fully occupied cells. Now, another relation holds: $N = (\kappa - q_0 - 1)\{0\} + 1\{n\} + q_0\{k^2\} \equiv n + q_0 k^2$, where $n = N \bmod k^2$, and $q_0 = (N - n)/k^2$, $q_0 \in (0, 1, \dots, \kappa - 1)$. The number of proper microstates is therefore

$$\Omega_{\min}(S) = \binom{k^2}{n} \binom{k^2}{k^2}^n \equiv \binom{k^2}{n}. \quad (A.4)$$

Now, we focus on the number $\Omega(G)$ of realizations of the actual macrostate $\text{AM}(G)$. The number of the appropriate compositional microstates is the product of the ways that each of sampled cells can be populated with the number k^2 of grey levels under above constraint (ii). Hence, the number of so-called weak compositions ([Stanley 2001](#)) is given by

$$\Omega(G) = \prod_{i=1}^{\kappa} \binom{g_i + k^2 - 1}{k^2 - 1}, \quad (\text{A.5})$$

where g_i denotes i th cell sum of grey level values.

The maximum possible value $\text{Entr}_{\max}(G)$ relates to most compositionally homogeneous reference macrostate, the $\text{RM}(G) = \{g_i \in (g_0, g_0 + 1)\}_{\max}$, with $\kappa - R_0$ and R_0 number of cells having local sums $g_0 \in (0, 1, \dots, 255k^2 - 1)$ and $g_0 + 1$ of grey levels. This leads to the simple expression: $G = (\kappa - R_0)\{g_0\} + R_0\{g_0 + 1\} \equiv \kappa g_0 + R_0$, where $R_0 = G \bmod \kappa$, $R_0 \in (0, 1, \dots, \kappa - 1)$ and $g_0 = (G - R_0)/\kappa$. Thus, the number of the proper microstates reads

$$\Omega_{\max}(G) = \binom{g_0 + k^2 - 1}{k^2 - 1}^{\kappa - R_0} \binom{g_0 + k^2}{k^2 - 1}^{R_0}. \quad (\text{A.6})$$

Finally, the minimum possible value $\text{Entr}_{\min}(G)$ is obtainable for most compositionally inhomogeneous reference macrostate, $\text{RM}_{\min}(G) \equiv \{g_i \in (0, g, 255k^2)\}_{\min}$, with $\kappa - Q_0 - 1$ cells having grey level sums equal to zero, one cell with $g_i = g \in (0, 1, \dots, 255k^2 - 1)$ and Q_0 cells with $g_i = 255k^2$. Then one can simply write: $G = (\kappa - Q_0 - 1)\{0\} + 1\{g\} + Q_0\{255k^2\} \equiv g + 255Q_0k^2$, where $g = G \bmod 255k^2$ and $Q_0 = (G - g)/255k^2$, $Q_0 \in (0, 1, \dots, \kappa - 1)$. Hence, the number of proper microstates is described by

$$\Omega_{\min}(G) = \binom{g + k^2 - 1}{k^2 - 1} \binom{255k^2 + k^2 - 1}{k^2 - 1}^{Q_0}. \quad (\text{A.7})$$

The above formulas contain the whole information we need to compute the corresponding entropy. In order to ease preparing of individual numeric program, I recommend a mathematical identity suitable to compute the logarithm of binomial coefficient; see [Van Siclen \(1997\)](#).

References

- Cule, D. & Torquato, S. 1999 Generating random media from limited microstructural information via stochastic optimization. *J. Appl. Phys.* **86**, 3428.
- Fullwood, D. T., Kalidindi, S. R., Niezgoda, S. R., Fast, A. & Hampson, N. 2008a Gradient-based microstructure reconstructions from distributions using fast Fourier transforms. *Mater. Sci. Engin. A* **494**, 68.
- Fullwood, D. T., Niezgoda, S. R. & Kalidindi, S. R. 2008b Microstructure reconstructions from 2-point statistics using phase-recovery algorithms. *Act. Mater.* **56**, 942.
- Fullwood, D. T., Niezgoda, S. R., Adams, B. L. & Kalidindi, S. R. 2009 Microstructure sensitive design for performance optimization. *Prog. Mater. Sci.* (doi: 10.1016/j.pmatsci.2009.08.002)
- Jiao, Y., Stillinger, F. H. & Torquato, S. 2007 Modeling heterogeneous materials via two-point correlation functions: I. Basic principles. *Phys. Rev. E* **76**, (the I part) 031110.
- Jiao, Y., Stillinger, F. H. & Torquato, S. 2008 Modeling heterogeneous materials via two-point correlation functions: II. Algorithmic details and applications. *Phys. Rev. E* **77**, (the II part) 031135.
- Jiao, Y., Stillinger, F. H. & Torquato, S. 2009 A superior descriptor of random textures and its predictive capacity. *PNAS* **106**, 17634.
- Kumar, H., Briant, C. L. & Curtin, W. A. 2006 Using microstructure reconstruction to model mechanical behavior in complex microstructures. *Mech. Mater.* **38**, 818.
- Lu, B. & Torquato, S. 1992 Lineal path function for random heterogeneous materials. *Phys. Rev. A* **45**, 922.
- Noussiou, W. K. & Provata, A. 2007 Surface reconstruction in reactive dynamics: A kinetic Monte Carlo approach. *Surf. Sci.* **601**, 2941.
- Patelli, E. & Schuëller, G. 2009 On optimization techniques to reconstruct microstructures of random heterogeneous media. *Comput. Mater. Sci.* **45**, 536.
- Piasecki, R. 2000a Entropic measure of spatial disorder for systems of finite-sized objects. *Physica A* **277** (1-2), 157.
- Piasecki, R. 2000b Detecting self-similarity in surface microstructures. *Surf. Sci.* **454-456**, 1058.
- Piasecki, R. 2009a Versatile entropic measure of grey level inhomogeneity. *Physica A* **388**, 2403.
- Piasecki, R. 2009b Statistical mechanics characterization of spatio-compositional inhomogeneity. *Physica A* **388**, 4229.
- Piasecki, R., Martin, M. T. & Plastino, A. 2002 Inhomogeneity and complexity measures for spatial patterns. *Physica A* **307**, 157.
- Piasecki, R. & Plastino, A. 2010 Entropic descriptor of a complex behaviour. *Physica A* **389**, 397.
- Rintoul, M. D. & Torquato, S. 1997 Reconstruction of the structure of dispersions. *J. Colloid Surface Sci.* **186**, 467.
- Rucklidge, A. M. & Silber, M. 2009 Design of parametrically forced patterns and quasipatterns. *SIAM J. Applied Dynamical Systems* **8**, 298.
http://www.maths.leeds.ac.uk/~alastair/papers/RS_gp_siads_example_12_to_14_anim.gif
- Stanley, R. P. 2001 *Enumerative Combinatorics*, vol. I. Cambridge University Press.
- Torquato, S. 2002a *Random Heterogeneous Materials: Microstructure and Macroscopic Properties*. Springer-Verlag.
- Torquato, S. 2002b Statistical description of microstructures. *Annu. Rev. Mater. Res.* **32**, 77.
- Torquato, S., Beasley, J. D. & Chiew, Y. C. 1988 Two-point cluster function for continuum percolation. *J. Chem. Phys.* **88**, 6540.
- Tsallis, C. 2009 *Introduction to Nonextensive Statistical Mechanics*. Springer-Verlag.
- Van Siclen, C. DeW. 1997 Information entropy of complex structures. *Phys. Rev. E* **56**, 5211.
- Wang, M. & Pan, N. 2008 Predictions of effective physical properties of complex multiphase materials. *Mater. Sci. Eng. R.* **63**, 1.
- Yeong, C. L. Y. & Torquato, S. 1998a Reconstructing random media. *Phys. Rev. E* **57**, 495.
- Yeong, C. L. Y. & Torquato, S. 1998b Reconstructing random media. II. Three-dimensional media from two-dimensional cuts. *Phys. Rev. E* **58**, 224.

Figure captions

Figure 1. (a) The unbiased hybrid reconstruction (UHR) making use of a pair of EDs, $\{S_{\Delta}; C_{\lambda, S}\}$, for a 36×36 simple binary pattern. The lines and symbols correspond to target pattern T #1 and its reconstruction R #1. (b) The restricted two-point correlation function S_2 of black phase computed by orthogonal-sampling algorithm for the two patterns, T #1 (solid line) and R #1 (dashed line), with the hard-wall conditions applied also for next figures. (c) The same but for exemplary 186×186 auxiliary patterns (see [Appendix](#)), auxT #1 (solid line) and auxR #1 (dashed line), which are created at the most characteristic length scale $k_{\max} = 6$.

Figure 2. (a) The UHR making use of a pair of EDs, $\{G_{\Delta}; C_{\lambda, G}\}$, for a modified 42×42 domain of three-level image presented in [Noussiou & Provata \(2007\)](#). The lines and symbols correspond to target pattern T #2 and its reconstruction R #2. For better visualisation of details we show only the EDs values larger than 1 and limit the length scales to $k \leq 23$. (b) From top to bottom, the S_2 -function (within the most interesting range of its values) of a white, grey and black phase computed for T #2 (solid lines) and R #2 (dashed lines).

Figure 3. The same as in [figure 2](#) but with interchanged white and grey phases. Likewise to the previous [figures 1b and 2b](#), in [figure 3b](#) the differences between solid and dashed lines are easily seen. Such behaviour may suggest that structural information given by correlation functions differs in part at least from that obtained with entropic descriptors. The comparable effect can be also observed in ensuing [figure 4b](#).

Figure 4. (a) The UHR making use of two pairs of EDs, $\{S_{\Delta}; C_{\lambda, S}\}$ and $\{G_{\Delta}; C_{\lambda, G}\}$, for a 64×64 sub-domain (left, upper corner) of the binary laser-speckle pattern adapted from [Jiao *et al.* \(2008\)](#) [with the permission of the authors]. The lines and symbols correspond to target pattern T #4 and its reconstruction R #4, respectively. For better visualisation of details we limit the length scales to $k \leq 32$. (b) The two-point correlation function S_2 of black phase computed by orthogonal-sampling algorithm for the two patterns, T #4 (solid line) and R #4 (dashed line). (c) The corresponding distribution of cluster sizes s (measured in pixels) for T #4 (black dropped lines) and R #4 (grey ones). The number $n(s)$ of clusters for $s > 22$ is given in [Table 1](#).

Figure 5. (a) The UHR making use of a pair of EDs, $\{G_{\Delta}; C_{\lambda, G}\}$, for an exemplary 137×137 sub-domain (resized then to 64×64) of greyscale intermediate pattern adapted from the animated movie of the transition between 12-fold and 14-fold approximated quasipatterns investigated in [Rucklidge & Silber \(2009\)](#) [with the permission of the authors]. The solid G_{Δ} -line and symbols correspond to target pattern T #5 and its reconstruction R #5 while the dashed line reeffers to the initial random configuration I #5. In the inset, the $C_{\lambda, G}$ -line hardly distinguishable from G_{Δ} -one is also shown around the first peak. (b) To facilitate comparison of patterns, the initial pattern I #5 (top), target one T #5 (middle) and its reconstruction R #5 (bottom) are depicted. In addition, the common grey level histogram is presented.

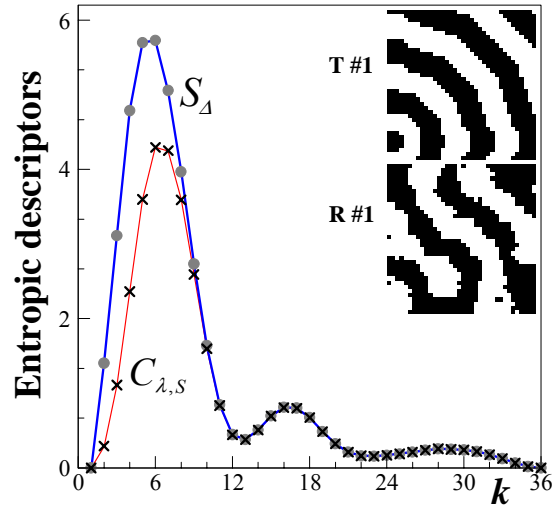


Figure 1a.

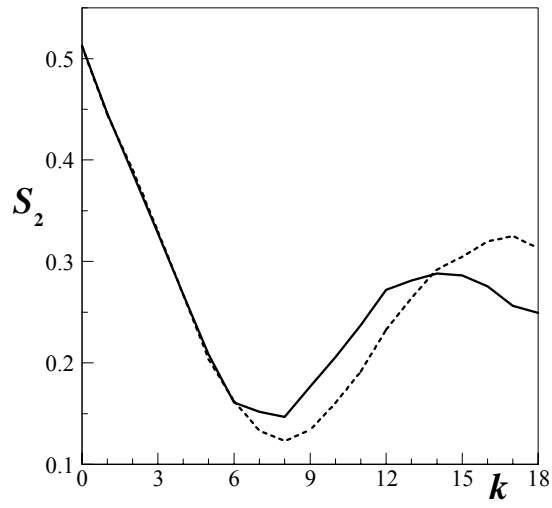


Figure 1b.

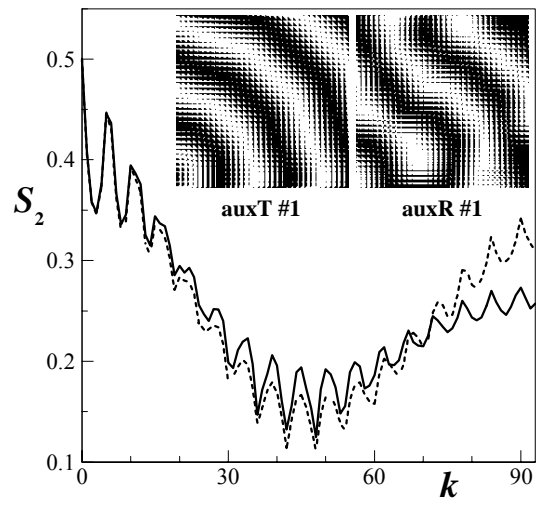


Figure 1c.

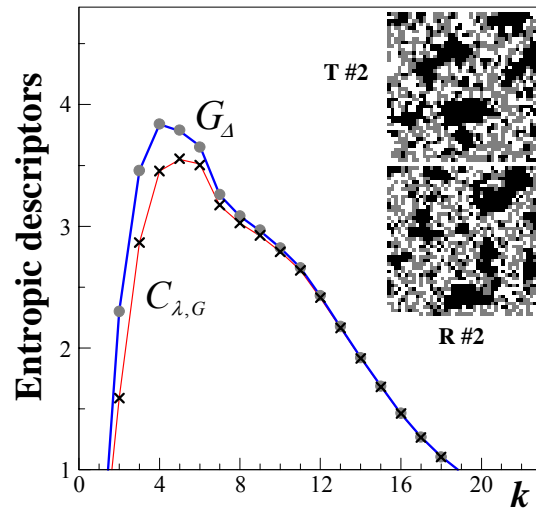


Figure 2a.

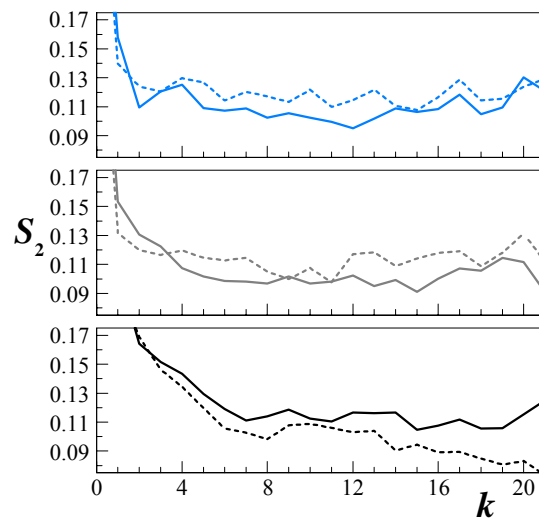


Figure 2b.

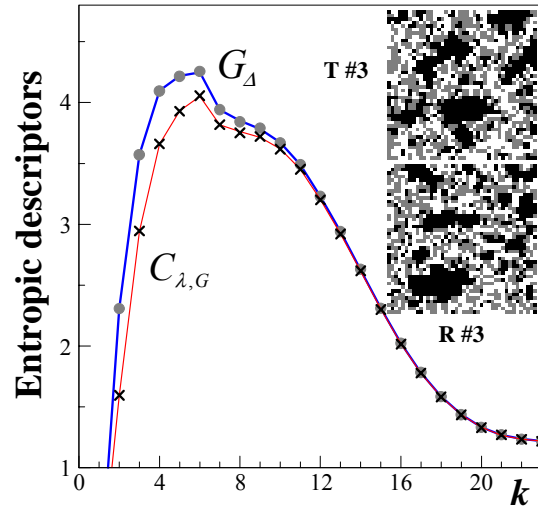


Figure 3a.

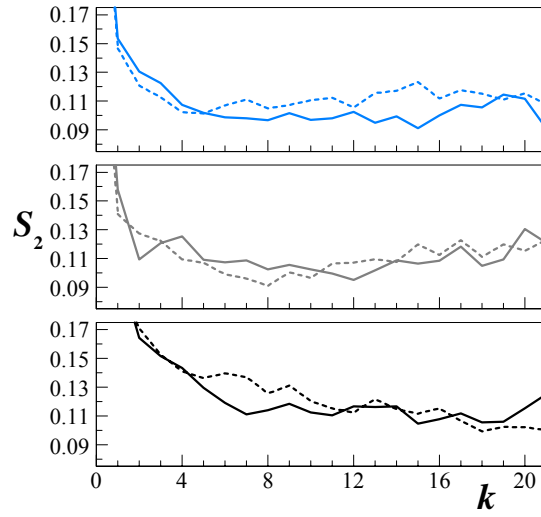


Figure 3b.

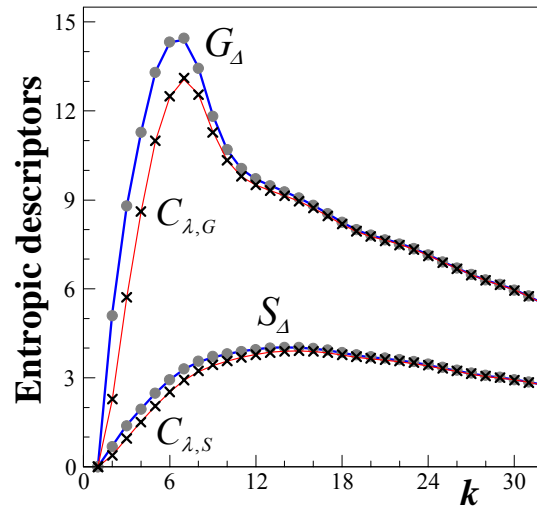


Figure 4a.

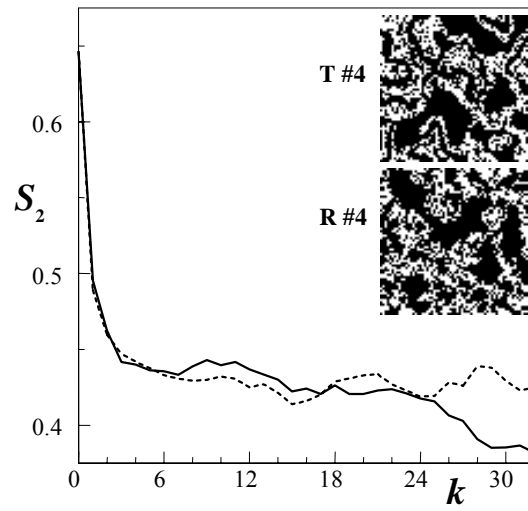


Figure 4b.

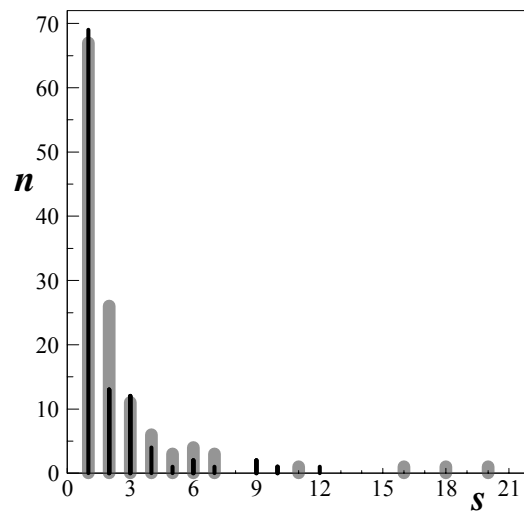


Figure 4c.

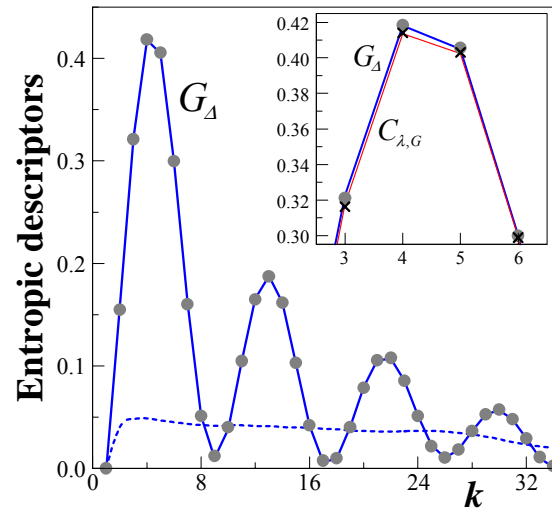


Figure 5a.

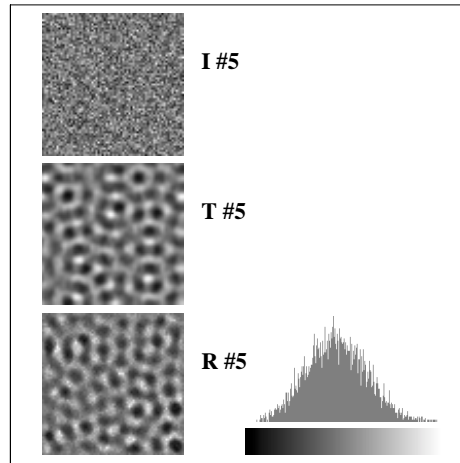


Figure 5b.